The role of interfacial strain in the surface p4g reconstruction: a comparison between Pd(001)–(2 × 2)p4g–Al and $Cu_3Pt(001)$

1997 J. Phys.: Condens. Matter 9 8345

(http://iopscience.iop.org/0953-8984/9/40/003)

J. Phys.: Condens. Matter **9** (1997) 8345–8358. Printed in the UK PII: S0953-8984(97)83814-3

The role of interfacial strain in the surface p4g reconstruction: a comparison between Pd(001)–(2 × 2)p4g–Al and Cu_3Pt(001)

Y G Shen†, D J O'Connor and R J MacDonald

Department of Physics, University of Newcastle, New South Wales 2308, Australia

Received 30 April 1997

Abstract. The surface composition and structure of the Pd(001)–(2 × 2)p4g–Al phase have been studied by low-energy ion scattering (LEIS) and low-energy electron diffraction (LEED). It was found that annealing Al-covered surfaces with initial coverages from half to larger than one monolayer (ML) to about 900 K gave rise to a stable (2 × 2)p4g LEED pattern. The ion scattering data suggest that the reconstruction is due to an ordered c(2 × 2) Al–Pd underlayer below a clock-rotated (001) Pd termination. To better understand the Pd(001)–(2 × 2)p4g–Al system, we have also studied an ordered Cu_3Pt(001) alloy surface, which exhibits the stable c(2 × 2) structure with an ordered c(2 × 2) Cu–Pt underlayer below a (1 × 1) Cu termination. Strain analysis shows that the top-layer reconstruction for the (2 × 2)p4g surface is caused by the Al-induced interfacial strain.

1. Introduction

The effects of mismatch stress caused by intermixing and thermal alloying at surfaces are important concerns in the growth of thin films on metal substrates. In particular, intriguing changes in the film structure and properties can be induced by subtle changes in the lattice strain. Many studies show that the lattice strain can be released either by formation of misfit dislocations [1, 2] or by a reconstruction of the respective layer(s) [3–5]. However, it is not fully understood whether the dramatic structural effects observed are due to charge-transfer-induced changes in the nature of the film or whether the effects are simply the result of lattice strain. In order to obtain a detailed understanding of the physical and chemical properties of thin films on metals, knowledge of the surface composition and structure of thin films at the surface is a prerequisite. This allows one to look at systematic difference between related systems, and also provides model systems against which theoretical calculations can be tested.

In this article, we present results of low-energy ion scattering (LEIS) and low-energy electron diffraction (LEED) studies of the interaction of Al with the Pd(001) surface. To the best of our knowledge, to date only the symmetry of the Pd(001)–(2 × 2)p4g–Al reconstruction has been reported [6]. Neither the composition nor the structure of the reconstructed surface has been established yet. The (2 × 2)p4g surface is formed when the initial deposited Al coverage is at least 0.5 ML but may be in excess of 1 ML upon annealing to ∼900 K. Our measurements unambiguously show that the thermal treatment of

† Corresponding author. Fax: +61 49 216907. E-mail address:phsy@cc.newcastle.edu.au

0953-8984/97/408345+14$19.50

the Al films triggers the Al diffusion and reaction which leads to the formation of an ordered c(2 × 2) Al–Pd underlayer below a clock-rotated (001) Pd termination, with a stoichiometry of the top two layers independent of the initial Al coverage. From the LEIS data and 3D computer simulation, the lateral displacement of the surface Pd atoms was determined to be $\Delta x = 0.5 \pm 0.1$ Å. A large buckling (0.25 ± 0.1 Å) of Al atoms in the c(2 × 2) Al–Pd underlayer has also been detected. Furthermore, comparisons are made with the behaviour of the analogous Cu_3Pt(001) surface, which does not show the reconstruction feature. The stoichiometry of the top two layers for the Cu_3Pt(001) surface was determined to be identical to the (2×2)p4g phase: an ordered c(2×2) Cu–Pt underlayer below a (1×1) Cu termination. Strain analysis indicates that the driving mechanism for the (2 × 2)p4g structure is caused by the Al-induced interfacial strain.

The main experimental techniques used were LEIS and LEED. LEIS has been well established as a probe for both surface composition and surface structure. This technique is therefore especially suited to investigating surface, interface and thin-film phenomena [7–10].

2. Experimental details

The experiments were carried out in a stainless-steel UHV chamber (7×10^{-11} mbar base pressure) equipped with an angle-resolved ion scattering system (VSW Scientific Instruments) and other facilities for surface characterization, i.e., LEED, Auger electron spectroscopy (AES), a Kelvin probe for work function measurements and a mass spectrometer for residual gas analysis [11]. The angle of incidence, α, measured from the surface plane, was calibrated by aligning an He–Ne laser along the ion beam direction. The azimuthal angle, ϕ, was measured from the [110] azimuths of clean Pd(001). The angle was initially determined by LEED measurements and then more finely adjusted using azimuthal angle ϕ scans in LEIS. The scattered ions were energy analysed by a hemispherical electrostatic analyser ($\Delta E/E = 0.02$), which is rotatable to allow variation of the total laboratory scattering angle Θ from 0 to 130°. The accuracies of the angles α, ϕ and Θ were ±0.5, 1 and 1° respectively. The analyser was equipped with a dual multichannel detector (MCD) to provide high count rates. The use of an MCD allows data collection with small ion doses to avoid any significant damage or desorption during the measurements.

The sample is a Pd crystal (12 mm in diameter and 1 mm thick) with a polished (001) surface from Commercial Crystal Laboratory (Techniches Büro). Final crystal cleaning was achieved by successive cycles of Ar^+ ion bombardment and annealing at ∼1050–1100 K. The carbon contamination was eliminated by several oxidation and reduction cycles. The well oriented (⩽0.5°) and polished Cu_3Pt(001) sample was cleaned by repeated cycles of Ar^+ ion bombardment (2 keV, 0.8 μA, 30 min) and annealing at 750–800 K. The temperature was measured by means of a chromel–alumel thermocouple and checked with an IR pyrometer. Surface cleanliness was verified by the absence of O, S and C from the He^+ LEIS spectra.

The Al deposition was carried out using resistively heated and collimated crucibles [12]. The Al coverage (Θ_{Al}) was determined by a quartz crystal microbalance (QCM) (Leybold INFLCON XTC), which was calibrated by ion scattering measurements [8, 13]. The evaporation rate was estimated to be accurate to ±15%. The source gave constant, reproducible and clean deposition of Al over long periods of time. During evaporation the pressure remained below 4×10^{-10} mbar. The Pd(001) substrate was held at room temperature (RT, 300–325 K) during Al deposition, LEED study and LEIS measurement. The Al was removed by Ar^+ ion bombardment after each measurement.

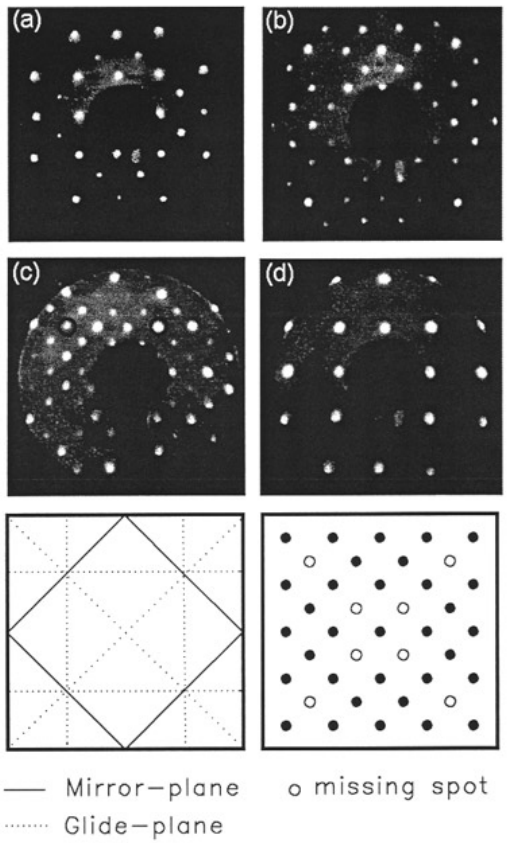

Figure 1. Typical LEED patterns corresponding to 1 ML Al on Pd(001) after annealing to 900 K for 3 min. (a)–(c) (2 × 2)p4g at (a) 71 eV and (b) 137 eV at normal beam incidence and (c) at 136 eV at 5° beam incidence. Spots of the type $(0, n + \frac{1}{2})$ are now visible and are circled. (d) c(2 × 2) at 65 eV. Below is a schematic LEED pattern with the indications of the missing spots shown together with the p4g space group symmetries.

3. Results

3.1. LEED studies

The clean Pd(001) surface exhibited a very sharp (1 × 1) LEED pattern with a low background. The initially sharp Pd(001) LEED pattern rapidly faded into a rising background as Al deposition commenced at RT, completely disappearing at $\Theta_{Al} = 0.5$ ML. This phenomenon can be understood as fractions of a monolayer of Al react with and displace Pd atoms in the whole surface selvedge and as a consequence completely destroy the LEED pattern. At Al deposition of 0.5 ML or greater upon annealing to ∼750–950 K for several minutes, the sharp (2 × 2)p4g LEED patterns were observed over a wide energy range from 35 to 200 eV. The sharp (2 × 2)p4g LEED patterns remained unchanged for Θ_{Al} from 0.5 to 4.7 ML. Further deposition after >4.7 ML was not studied. This is in good agreement with the observations reported in [6].

Figure 1(a) and (b) shows typical (2 × 2)p4g LEED patterns recorded with 1 ML Al

deposited at RT followed by annealing to 900 K for 3 min at two incident beam energies. The LEED pattern of the p4g reconstruction is in principle a (2×2) where every spot labelled $(0, n+\frac{1}{2})$ or $(n+\frac{1}{2}, 0)$ is absent at normal electron beam incidence, while they become visible upon rotation of about 5° around the [001] direction (figure 1(c)). In addition, a sharp c(2×2) pattern was also observed at certain beam energies (figure 1(d)), suggesting the existence of a separate c(2×2) phase. Our ion scattering results shown below indicate that this separate c(2×2) phase is a mixed Al–Pd underlayer. For the (2×2)p4g structure, we also detected no change of the positions of the integral order spots (at fixed energy), revealing that the dissolution of Al in Pd upon annealing has no effect on the Pd substrate lattice. Upon heating the surface to higher temperature ($\sim$1100 K) the (2×2)p4g pattern changed to a sharp (1×1) pattern of the clean Pd(001) surface due to Al diffusion into the bulk.

3.2. A clock-rotated (001) Pd top layer for the (2× 2)p4g structure

Since LEIS with He^+ ions is an extremely surface-sensitive method with virtually no signal contributed by the second or deeper layers of a surface, it is an ideal technique for the determination of the stoichiometry of the reconstructed surface. Figure 2 shows typical energy spectra of He^+ ion scattering from clean Pd(001) and several Al depositions before and after an anneal to 900 K. As Al is deposited, the Al single-scattering intensity increases, while the reverse trend is seen for the Pd single-scattering intensity. In all cases both peaks appear near the kinetic energy values expected from the binary collision approximation model [7]: 928 eV for Pd and 742 eV for Al. At 1 ML coverage, the spectrum from the unannealed film shows that about 95% of the substrate is covered. An important feature of figure 2 is that after annealing the surface to 900 K the Al single-scattering intensity is no longer detectable, independent of the initial Al coverage. This is due to the fact that annealing the Al films to this temperature provides sufficient atomic mobility for Al atoms to diffuse into the substrate. The fact that the Pd single-scattering intensity for the (2×2)p4g surface is essentially the same as for the clean Pd(001) surface reveals that the surface density of the (2×2)p4g structure is identical to that of Pd(001).

On a day to day basis, it was found that the (2×2)p4g reconstruction was readily produced and very reproducible when the Al films ($\Theta_{Al}\geqslant0.5$ ML) were deposited at RT, and annealed to $\sim$900 K leading to the formation of a clock-rotated (001) Pd top layer. The azimuthal angle ϕ scan in ion scattering is well suited for demonstrating this fact. Figure 3(a) and (b) shows energy and angle dispersive LEIS distributions (raw data) of the ϕ scans at grazing incidence, collected from the clean Pd(001) and (2×2)p4g surfaces, respectively. The integrated Pd intensities as a function of ϕ are shown in figure 4. Included with the data are also simulations of the ϕ scans from the Pd(001) and (2×2)p4g surfaces. The proposed model for the clock reconstruction is shown above the figure, which includes a simple (001) Pd overlayer with the p4g symmetry above an ordered c(2×2) Al–Pd underlayer.

For the clean Pd(001) surface, the deep and wide minima centred at $\phi=0$ and 45° indicate the short interatomic spacings between surface Pd atoms in the [100] and [110] azimuths. The shallow and narrow minima at around $\phi=-18$ and 18° result from the next shortest interatomic spacings along the $[3\bar{1}0]$ and [310] azimuths. The agreement between the experimental and simulated shadowing dips confirms the (1×1) structure of the Pd(001) surface. Annealing the Al film to 900 K gives rise to different shadowing features from those observed for the clean Pd(001) surface: the disappearance of the shadowing dip at around $\phi=0^\circ$ is a result of several first-layer Pd–Pd interatomic spacings, some of which

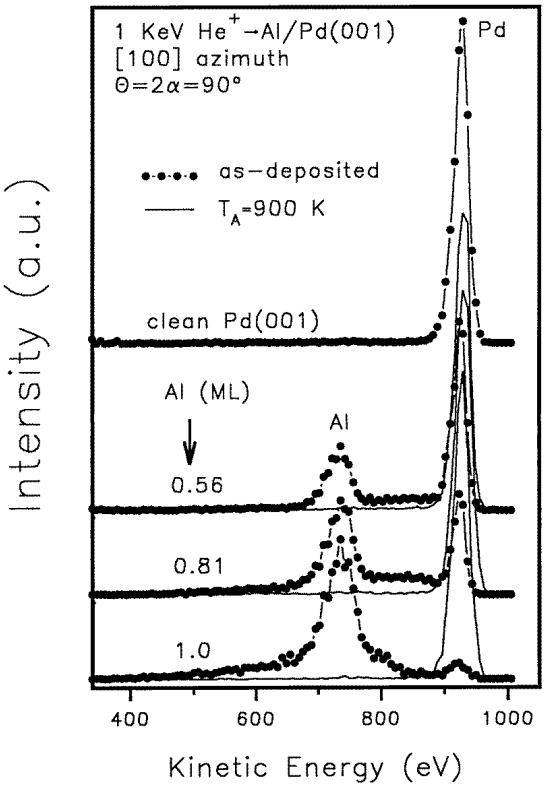

Figure 2. Energy spectra obtained from the clean Pd(001) and several Al depositions before and after an anneal to 900 K for 3 min using 1 keV He^+ ions ($\Theta = 2\alpha = 90^\circ$) along the [100] azimuth.

are double that of the unreconstructed surface causing no Pd–Pd alignments short enough to cast shadowing effects along the [100] azimuth. The main shadowing dip along the [110] azimuth at $\phi = 45^\circ$ becomes less pronounced, indicating that first-layer Pd–Pd nearest-neighbour atoms are not best aligned. The fact that the shadowing dips at around $\phi = -18$ and 18° are more pronounced compared to those from the clean Pd(001) surface could be interpreted as a result of efficient shadowing caused by the lateral movement of Pd atoms from their original positions along the $[3\bar{1}0]$ and [310] directions.

For the (2×2)p4g surface, the agreement between the experimental and simulated ϕ scans was judged on the basis of the reliability R factor [14, 15]. Simulations for the (2×2)p4g surface were carried out as a function of the Pd lateral displacement (Δx) from 0.1 to 1.0 Å in steps of 0.1 Å. R factors were calculated for comparison of each of the simulated ϕ scans with the experimental data. The best fit to the experimental data was achieved with the minimum R factor of $R = 0.090$ at $\Delta x = 0.5\pm0.1$ Å. Repeated measurements involving several different Al coverages between 0.5 and 4.7 ML upon annealing over several months showed that the minimum in R factors was reproducible to within $\pm15\%$. This geometrical parameter of the reconstruction has been further confirmed by using the R-factor analysis to compare the experimental and simulated ϕ scans using both Li^+ and K^+ ions.

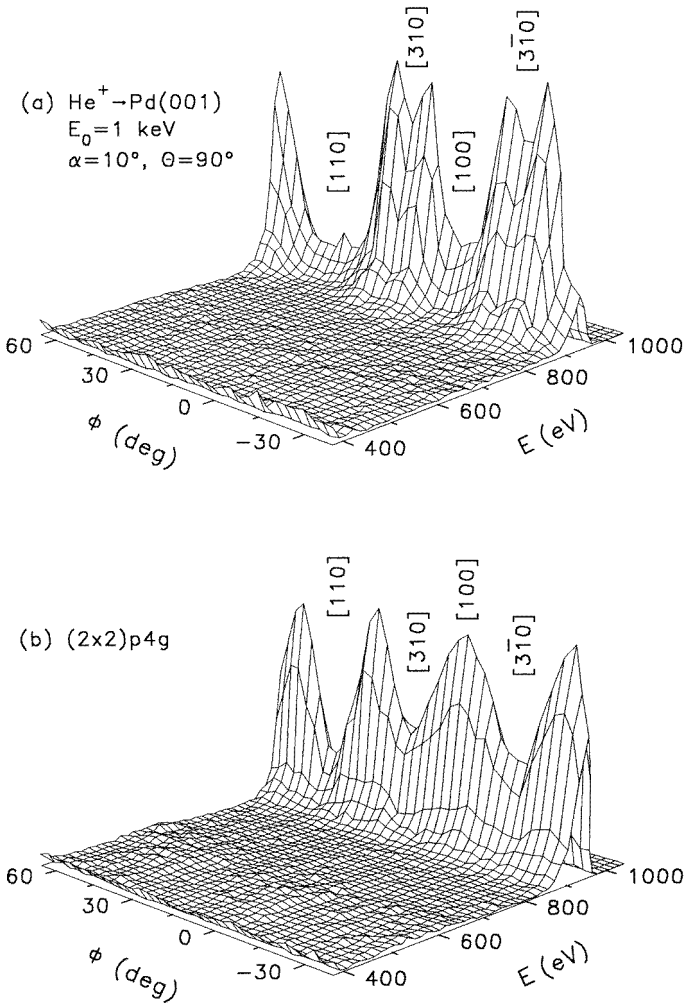

Figure 3. Experimental LEIS energy and angle dispersive backscattered intensity distributions obtained from (a) the clean Pd(001) surface and (b) the (2×2)p4g surface (0.8 ML Al, $T_A = 900$ K for 3 min) with 1 keV He^+ ions at $\alpha = 10^\circ$ and $\Theta = 90^\circ$.

3.3. Al buckling in the c(2× 2) Al–Pd underlayer for the (2× 2)p4g structure

In order to detect whether any Al atoms diffused into the second layer upon annealing, typical energy spectra are shown in figure 5(a) for the (2×2)p4g surface measured in the [210] azimuth for two different incident angle conditions using 5 keV Ne^+ ions. At an incident angle of $\alpha = 18^\circ$, the scattering under this geometry is dominated by first-layer scattering. The results indicate that Al is completely depleted from the top layer, in agreement with the results derived using He^+ ions. Information from the second layer was obtained from scattering along the same azimuth, but at a higher incident angle of 37°, where second-layer Al atoms have emerged from shadow cones of the first-layer Pd atoms. Using a scattering angle of $\Theta = 130^\circ$, all single scattering from the third layer and below is

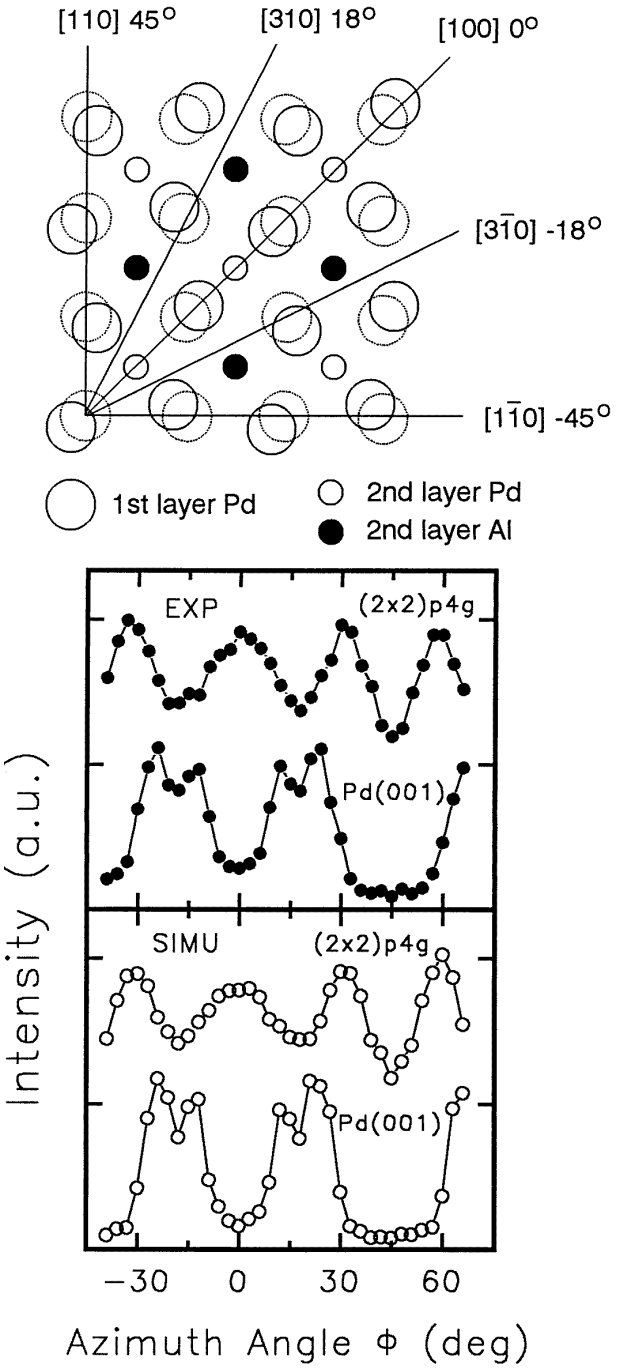

Figure 4. A comparison between the experimental (from figure 3 with solid circles) and simulated (open circles) azimuthal ϕ scans. The (2×2)p4g surface used for the simulations was constructed by a clock-rotated (001) Pd layer above a c(2×2) Al–Pd underlayer. Simulated parameters were the ZBL potential, surface Pd Debye temperature 270 K, $\Delta x = 0.5$ Å, and 160 000 incident projectiles. The proposed schematic model of the (2×2)p4g structure is shown at the top of the figure. The alignment directions are indicated.

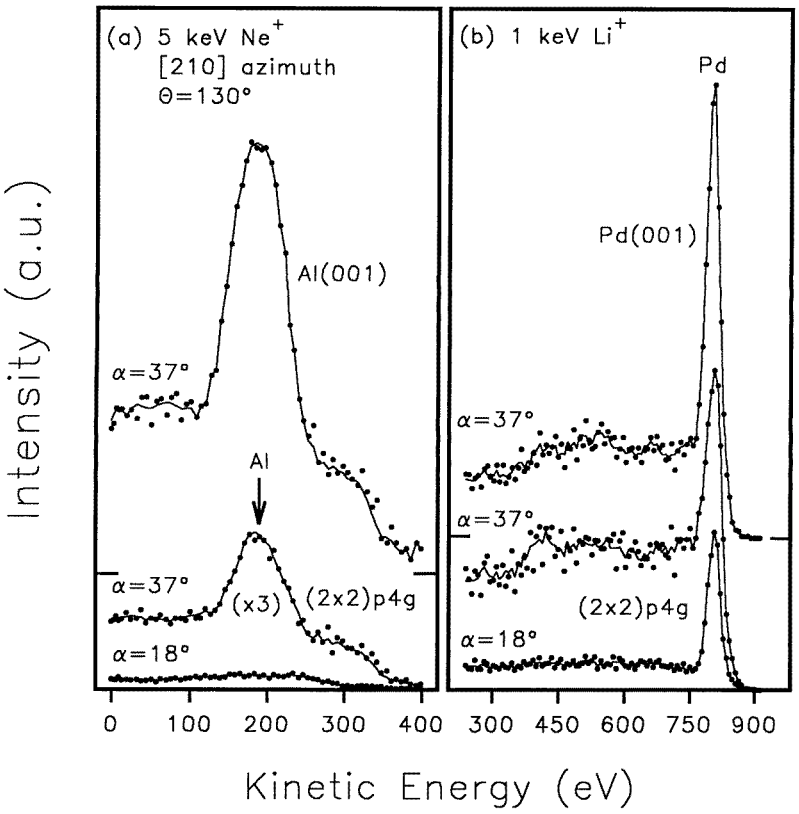

Figure 5. Energy spectra obtained from the (2×2)p4g surface for two different incident angle conditions using (a) 5 keV Ne^+ and (b) 1 keV Li^+ ions. The spectra obtained from the reference samples of Al(001) and Pd(001) have also been included, respectively. The intensities have been normalized to the beam current. The Al(001) (also Pd(001)) and (2×2)p4g curves have been offset for clarity.

blocked under this geometry. From the Ne results in figure 5(a), a new Al single-scattering peak at beam kinetic energy $\sim$ 190 eV is observed, indicating the presence of substantial quantities of Al in the second layer. Similarly equivalent information for the Pd signals in the top two layers was obtained using 1 keV Li^+ ions shown in figure 5(b). We should point out that Al single-scattering peaks from the second layer are superimposed on a large background signal at lower kinetic energies owing to multiple, inelastic scattering of the Li^+ ions from the subsurface. Such a background totally obscures the LEIS Al peak (at $\sim$420 eV) (see figure 5(b)). Using a simple shadow cone analysis with calibration measurements on reference Al(001) and Pd(001) standards, the Al and Pd compositions in the second layer were independently determined to be $45\pm$ 8% and $53\pm$ 6%, respectively. The quoted errors reflect the magnitude of random scatter based on many independent measurements.

The measured Al and Pd concentrations in the second layer were obtained after repeated deposition followed by annealing over a period of several months. Further measurements indicate that initial deposits in excess of 0.5 ML, upon annealing always evolved into a (2×2)p4g structure with identical Al concentrations in the second layer. The ion scattering data presented here cannot determine the ordering of the Al–Pd underlayer, but our LEED

patterns certainly suggest the ordering of the underlying c(2 × 2) structure. This is based on the observation of more intense ($\frac{1}{2}$, $\frac{1}{2}$) order spots over a wide energy range in the LEED pattern and is further supported by the fact that a sharp c(2 × 2) pattern is also observed at certain beam energies (see figure 1(d)).

In principle, it is possible to determine the first interlayer spacing for the (2 × 2)p4g surface by setting the scattering plane along a row containing the shadowing critical angle α_c associated with scattering from the second layer [9–11]. Data shown in figure 6 show the incident angle α scans from the Al(001) surface and the (2 × 2)p4g surface measured in the [210] azimuth at $\Theta = 130^\circ$ using 5 keV Ne^+ ions. For the Al(001) surface, the intensity increase of the single-scattering shadowing edge A (as measured at 80% height [16]) at about $\alpha_c \approx 7^\circ$ results from first-layer Al atoms. The second shadowing edge B at $\alpha_c \approx 34^\circ$ is attributed to first-layer Al atoms focusing onto second-layer Al atoms. Once again, at $\Theta = 130^\circ$ all single scattering from the third layer and below is blocked near the second shadowing edge. We also note that the signal originating from the second layer is reduced by a factor of approximately four relative to the first-layer signal at $\alpha \approx 18^\circ$, mainly due to the higher neutralization rate for Ne^+ ions backscattered from the second layer [10]. For the (2 × 2)p4g surface, annealing causes a disappearance of the Al signal in the top layer (at the lower α angles) and the appearance of the edge B at higher incident angle ($\alpha_c \approx 35^\circ$). In order to determine the first interlayer spacing, a 3D computer simulation for calculating the α scan has been performed to compare with the experimental α scan. We used the ZBL potential for the description of Li–Pd and Li–Al interactions. The first interlayer spacing, d_{12}(Pd–Al), was varied from 1.6 to 2.4 Å. The lateral displacement of surface Pd atoms was fixed to be 0.5 Å. The step widths in the calculation were 0.05 Å. The comparison between the experimental critical angle and the calculated one indicates that $d_{12}(\text{Pd–Al}) = 1.70 \pm 0.1$ Å, which reveals a large contraction of 13% of the first interlayer spacing (bulk value 1.946 Å). Similarly using 1 keV Li^+ ions at $\Theta = 130^\circ$ the first interlayer spacing, d_{12}(Pd–Pd), was measured to be 1.95 ± 0.05 Å (bulklike) (not shown). We conclude that the Al atoms in the c(2 × 2) underlayer were vertically buckled outward by 0.25 ± 0.1 Å.

3.4. (1× 1) Cu termination above the c(2× 2) Cu–Pt second layer for Cu_3Pt(001)

Cu_3Pt single-crystal alloy has a typical Cu_3Au ($L1_2$) structure. Below the critical temperature of the order–disorder transition of the crystal (∼870 K [17]), two truncated surface terminations of a Cu_3Pt(001) surface are possible: one is an ordered outermost layer of Cu–Pt stoichiometry, and the other is the pure Cu termination. Our LEED result shows the c(2 × 2) pattern of a clean Cu_3Pt(001) surface by annealing to a temperature at ∼800 K. No impurities were detected by low-energy He^+ ion scattering.

After cleaning by Ar^+ sputtering the Cu_3Pt(001) surface was annealed by heating gradually up to 800 K. During this heating period a large change in the Pt/Cu intensity ratio was observed. Finally the depletion of Pt in the top layer was observed. Figure 7 shows a series of energy spectra taken from the clean and well annealed Cu_3Pt(001) surface using 500 eV He^+ ions. These observations immediately lead to the conclusion that the clean and well annealed Cu_3Pt(001) surface has a pure Cu termination. Further annealing the Cu_3Pt(001) at 800 K for times of up to several hours caused no further change in the Cu intensity.

The second-layer composition of the Cu_3Pt(001) surface was determined using 1 keV Li^+ ions under selective scattering geometrical conditions where only the first-layer or where a sum of first- and second-layer scattering is observed. Typical energy spectra taken from

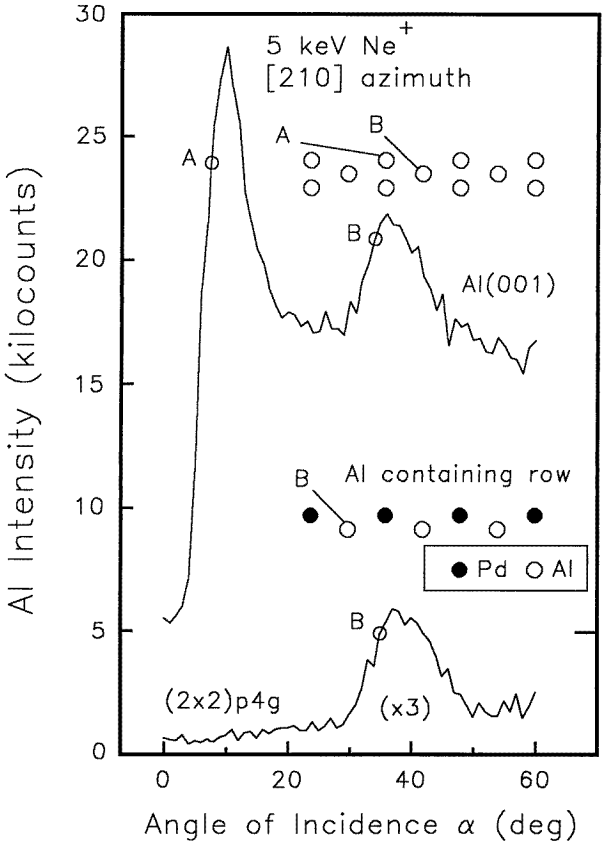

Figure 6. Incident angle α scan (in 1° intervals) of the integrated Al single-scattering intensities obtained from the (2×2)p4g surface (1 ML, $T_A = 900$ K for 3 min) in the [210] azimuth at $\Theta = 130^\circ$ is compared for a clean Al(001) surface using 5 keV Ne^+ ions. The intensities have been normalized to the beam current. The critical angles α_c are indicated by open circles.

the $Cu_3Pt(001)$ surface for two geometrical conditions are shown in figure 8. With the beam at an incident angle (α) of 45° along the [100] azimuth, single scattering can only occur from atoms in the top atomic layer since sub-surface atoms are completely shadowed and blocked by the first-layer atoms for this geometry. In order to observe single scattering from both the first and second layers, while shadowing deeper layers, the beam was incident at $\alpha = 35^\circ$ in the [110] azimuth. Since the $Cu_3Pt(001)$ surface has a pure Cu termination, this makes calibration of the LEIS first-layer signal and determination of the focusing factor easy [9, 16]. Under thermal equilibrium conditions, our results consistently showed the composition of 48% Pt–52% Cu in the second layer within an uncertainty of about $\pm 6\%$, in good agreement with the $c(2 \times 2)$ LEED structure observed. The value is the average of four different measurements under several different scattering angles ($\Theta = 90$, 100, 110 and 130°) and the error corresponds to the value of standard deviations. For details of this determination procedure as well as the calculation method, see a similar approach used on $Cu_3Pt(111)$ reported previously [16]. The measured composition of the top two layers was obtained from the clean and well annealed $Cu_3Pt(001)$ surface over a period of several weeks. We suggest that an ordered $c(2 \times 2)$ Cu–Pt underlayer below a Cu (1×1) termination

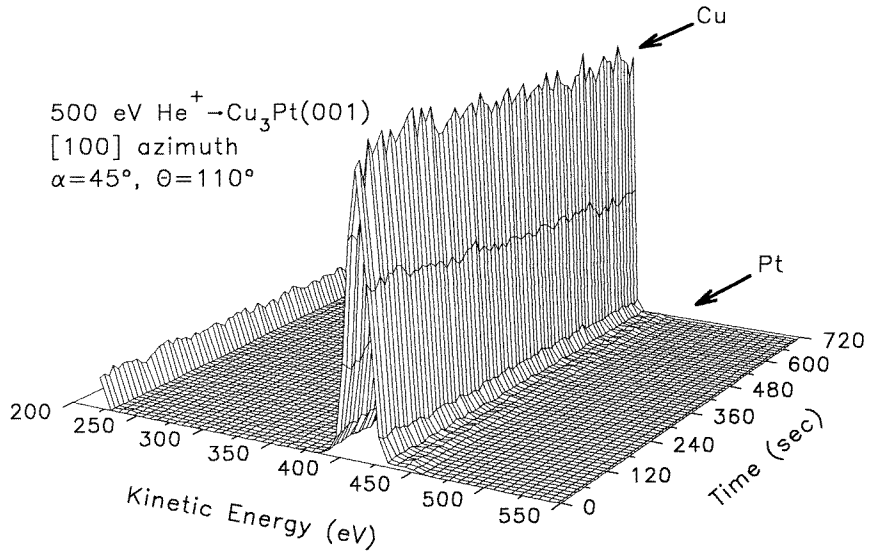

Figure 7. Energy spectra collected from the clean and well annealed $Cu_3Pt(001)$ surface using 500 eV He^+ ions (the time for collecting each spectrum is 10 s).

is a thermal equilibrium configuration.

We have measured the Cu and Pt α scans along the [210] azimuth at $\Theta = 130^\circ$ using Li^+ ions with three different beam energies (0.5, 1.0 and 1.5 keV) (not shown). Using the same approach for the determination of the first interlayer spacing for the (2×2)p4g structure as described in section 3.3, the first interlayer spacing of the $Cu_3Pt(001)$ surface, d_{12}, was determined to be 1.80 ± 0.06 Å (bulk value 1.85 Å) corresponding to a small contraction of $-2.7 \pm 1.2\%$. The results also indicate that the Cu and Pt atoms are in the same plane of the (2×2) Cu–Pt second layer within an uncertainty of ± 0.05 Å. The details of the experimental α scans and structural determination for the $Cu_3Pt(001)$ surface will be reported in a future publication.

4. Discussion

The lower surface energy of Al compared to Pd restricts Al to wet the surface at RT but by annealing a clock-rotated pure Pd layer is produced with exclusion of Al by diffusion of Al into Pd rather than by outward diffusion of Pd. The annealing used in the present investigation presumably serves only to activate atom diffusion, place exchange and structure conversion. The observation that thermally induced mixing occurs in the interfacial layer is not very surprising in view of the fairly high solubility of Al in Pd and the fact that several intermetallic compounds form between Al and Pd [18]. The more interesting result is that upon annealing to 750–950 K (about 0.39–0.5 T_m, where T_m is the melting temperature of the substrate) the surface readily forms a clock-rotated Pd layer above a mixed $c(2 \times 2)$ underlayer with Al coverage of 0.5 ML. The surface reaches this state by rapid dissolution of excess Al (i.e., amounts larger than 0.5 ML) into the bulk. These observations suggest that the higher solubility of Al in Pd facilitates the process of dissolving excess Al (with a time scale on the order of several minutes) into the bulk at these temperatures, although the depth profile of Al is unknown. The resulting clock-rotated (001) Pd top layer and

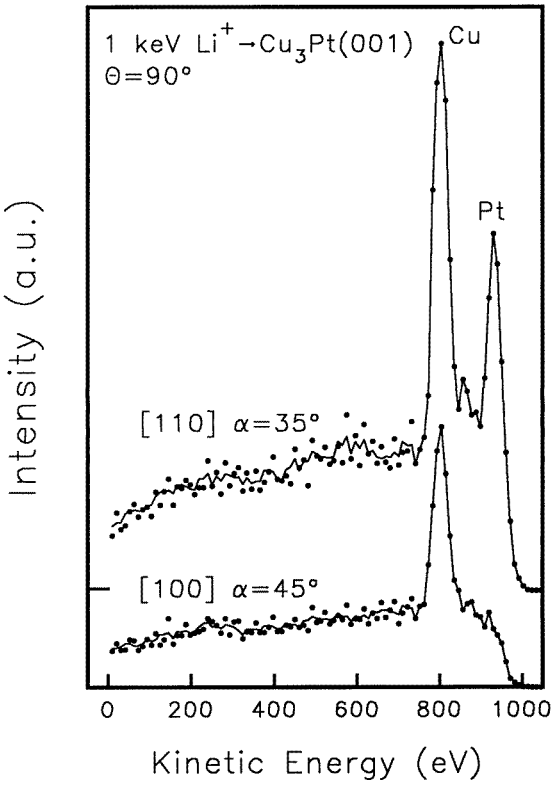

Figure 8. Energy spectra obtained from the clean and well annealed $Cu_3Pt(001)$ surface using 1 keV Li^+ ions for two different geometrical conditions.

a c(2 × 2) underlayer are then quite stable against Θ_{Al} changes, depth redistributions or interfacial reordering.

The Al–Pd phase diagram indicates that the formation of the bulk compound β-AlPd with the CsCl structure is thermodynamically favourable [18]. However, this structure was not observed. When we observe the (2 × 2)p4g phase upon annealing, the system may not have yet reached its equilibrium structure. The fact that the (2 × 2)p4g phase appears over such a broad coverage range may be due to the fact that it is kinetically prevented from converting to β-AlPd, or that the surface (2 × 2)p4g structure is more stable. We suggest that the (2 × 2)p4g phase is not characteristic of any bulk intermetallic compounds and therefore seems to be uniquely associated with an interfacial phase. It is expected [19] that equilibration of the surface by interdiffusion occurs in a reasonable time scale only above $\sim\frac{2}{3}$ of the melting temperature (T_m = 1918 K [18]), so we should not be surprised that β-AlPd is not formed here at 0.39–0.5 T_m.

Comparisons between the (2 × 2)p4g surface and the $Cu_3Pt(001)$ surface have also been made. Our LEED and ion scattering results indicate that the clean and well annealed $Cu_3Pt(001)$ surface has a long-range-ordered structure (an ordered c(2 × 2) Cu–Pt underlayer below a (1 × 1) Cu termination) which does not show reconstruction behaviour. As the stoichiometries of the top two layers for these two systems are similar, the only apparent cause of the structural difference is a large buckling in the c(2 × 2) Al–Pd underlayer for the

(2×2)p4g surface while no buckling in the c(2×2) Cu–Pt second layer for the $Cu_3Pt(001)$ surface. The buckling is attributed to relief of strain created by incorporating the large Al atoms. That such similar systems produce such different structural behaviour would seem to be an indication of the delicate balance between the factors governing strain relief in surface layers.

Thus from these comparisons the driving force for the clock-rotated structure can be understood. The Al atoms in the underlayer are under considerable compressive stress due to the ∼4.5% lattice mismatch between Al and Pd. This strain is relieved by buckling with relaxed Pd–Al interlayer spacing. The large buckling of 0.25 Å observed for Al incorporated into the underlayer must exert a force on the top layer. Therefore, top-layer neighbouring Pd atoms share in a collective way the cost of inducing a p4g clock reconstruction in which the squares of Pd atoms surrounding the underlying ripple Al atoms rotate laterally. This produces two perpendicular glide symmetry lines along the directions of the missing spots and leads to the experimentally observed systematic extinction of $(0, n + \frac{1}{2})$ and $(n + \frac{1}{2}, 0)$ LEED spots at normal incidence. Energetically, the atoms in the reconstructed surface therefore experience an energy reduction via two related effects: (i) by reducing in-plane strain energy through buckling of larger atoms but creating a large interfacial strain, and (ii) by lowering the surface energy to trigger the clock rotation thereby relieving the interfacial strain. In any case, strain relief is playing an important role in the formation and stability of the reconstruction. However, whether or not charge transfer from underlayer Al to the top-layer Pd because of the lower electronegativity of Al also plays a role in the reconstruction of the (2×2)p4g surface remains an open question at present.

5. Conclusion

We have demonstrated that for sub-monolayer Al coverages ($\Theta_{Al} \geqslant 0.5$ ML) deposited at RT, annealing to ∼900 K gave rise to a stable (2×2)p4g reconstruction with a clock-rotated (001) Pd top layer above an ordered c(2×2) Al–Pd underlayer. The driving mechanism for the reconstruction is that the Al-induced interfacial strain is relieved by distorting (reconstructing) the top layer from its perfect crystal lattice positions. The difference between the (2×2)p4g phase and the $Cu_3Pt(001)$ structure (both have the c(2×2) underlayer below a pure (1×1) termination) may be a direct consequence of lattice strain. While the (2×2)p4g phase is under considerable compressive interfacial strain, the alloy is nearly strain free. To further correlate the ability to induce reconstruction with mixing and thermal alloying, more extensive systematic studies are needed. Experimentally, this (2×2)p4g reconstruction needs further experimental verification by a complementary experimental technique such as scanning tunnelling microscopy and full dynamical LEED I–V analysis. It would also be of interest to study how the stability of the reconstruction depends upon bulk composition up to the Al solubility limit.

Acknowledgments

The financial support of this work by the Australian Research Council is gratefully acknowledged. The authors are grateful to Dr J Yao for the contributions made in the early stages of this study and for many stimulating discussions. We are also indebted to Professor K Wandelt for providing us with the $Cu_3Pt(001)$ crystal.

References

[1] Stevens J L and Hwang R Q 1995 *Phys. Rev. Lett.* **74** 2078
[2] Hahn E, Kampshoff E, Wälchli N and Kern K 1995 *Phys. Rev. Lett.* **74** 1803
[3] Woodruff D P 1994 *The Chemical Physics of Solid Surfaces* vol 7, ed D A King and D P Woodruff (Amsterdam: Elsevier) ch 12
[4] Bardi U 1994 *Rep. Prog. Phys.* **57** 939
[5] Murray P W, Stensgaard I, Lægsgaard E and Besenbacher F 1996 *Surf. Sci.* **365** 591
[6] Onishi H, Aruga T and Iwasawa Y 1993 *Surf. Sci.* **283** 213
[7] Niehus H, Heiland W and Taglauer E 1993 *Surf. Sci. Rep.* **17** 213
[8] Diebold U, Pan J M and Madey T E 1993 *Phys. Rev.* B **47** 3868
[9] Overbury S H, van den Oetelaar R J A and Zehner D M 1993 *Phys. Rev.* B **48** 1718
[10] Detzel Th, Memmel N and Fauster Th 1993 *Surf. Sci.* **293** 227
[11] Shen Y G, Yao J, O'Connor D J, King B V and MacDonald R J 1995 *J. Phys.: Condens. Matter* **8** 4903
[12] Wytenberg W J and Lambert R M 1992 *J. Vac. Sci. Technol.* A **10** 3597
[13] Shen Y G, O'Connor D J, van Zee H, Wandelt K and MacDonald R J 1995 *Thin Solid Films* **263** 72
[14] Copel M and Gustafsson T 1986 *Phys. Rev.* B **33** 8110
[15] Ahn J, Bu H, Kim C, Bykov V, Sung M M and Rabalais J W 1996 *J. Phys. Chem.* **100** 9088
[16] Shen Y G, O'Connor D J, Wandelt K and MacDonald R J 1995 *Surf. Sci.* **328** 21
[17] Hansen M and Ander K 1958 *Constitution of Binary Alloys* (New York: McGraw-Hill)
[18] McAlister A J 1987 *Bull. Alloy Phase Diagrams* **7** 368
[19] Campbell C T 1990 *Annu. Rev. Phys. Chem.* **41** 775